Editors' Suggestion

Magnetic order in the van der Waals magnet VCl_3

Zeyu Kao,[1] Yiqing Hao,[2] Yimeng Gu,[1] Lixing Chen,[1] Enkang Zhang,[1] Hao Zhang,[1] Fabio Orlandi,[3] Pascal Manuel,[3] Junfeng Wang,[4] Chao Dong,[4] Chuanying Xi,[5] Zefeng Chen,[6] Changsong Xu,[6] and Jun Zhao[1,7,*]

[1]*State Key Laboratory of Surface Physics and Department of Physics, Fudan University, Shanghai 200433, China*

[2]*Neutron Scattering Division, Oak Ridge National Laboratory, Oak Ridge, Tennessee 37831, USA*

[3]*ISIS Pulsed Neutron and Muon Source, Science and Technology Facility Council, Rutherford Appleton Laboratory, Harwell Campus, Didcot OX11 0QX, United Kingdom*

[4]*Wuhan National High Magnetic Field Center and School of Physics, Huazhong University of Science and Technology, Wuhan 430074, China*

[5]*Anhui Key Laboratory of Low-Energy Quantum Materials and Devices, High Magnetic Field Laboratory, HFIPS, Chinese Academy of Sciences, Hefei, Anhui 230031, China*

[6]*Key Laboratory of Computational Physical Sciences (Ministry of Education), Institute of Computational Physical Sciences, State Key Laboratory of Surface Physics, and Department of Physics, Fudan University, Shanghai 200433, China*

[7]*Institute of Nanoelectronics and Quantum Computing, Fudan University, Shanghai 200433, China*

(Received 9 October 2025; revised 4 February 2026; accepted 20 February 2026; published 13 March 2026)

We investigated the structural and magnetic properties of single-crystalline VCl_3, a newly synthesized member of the vanadium trihalide family. High-quality single crystals were grown by the chemical vapor transport method, and their behavior was characterized using neutron diffraction and thermodynamic measurements. We show that VCl_3 crystallizes in the BiI_3-type structure at room temperature and undergoes a structural phase transition at $T_S = 103.7(5)$ K that lowers the lattice symmetry, followed by a zigzag antiferromagnetic order with a propagation vector $k = (0,\ 0.5,\ 1)$ below $T_N = 21.8(1)$ K. Neutron diffraction experiments indicate that the ordered moments are canted by approximately 21° away from the c axis toward the a axis, yielding a total moment of approximately $1.09(2)\mu_B/V^{3+}$. Field-dependent magnetization along the c axis exhibits a half magnetization plateau, indicative of a field-stabilized fractional state. These results establish VCl_3 as a new platform for exploring structural transitions, anisotropic magnetism, and field-induced phases in vanadium-based honeycomb magnets.

DOI: 10.1103/fj11-mwxv

I. INTRODUCTION

Layered van der Waals magnets have recently attracted significant attention due to their potential applications in spintronic and magneto-optic devices, as well as their fundamentally intriguing physics [1–5]. Among these two-dimensional (2D) materials, binary transition-metal trihalides TX_3 (T = transition metal; X = Cl, Br, I) have emerged as a focal point in the study of low-dimensional magnetism owing to their rich variety of magnetic ground states. Within this family, compounds such as VI_3 [6–8] and CrI_3 [9,10] have been confirmed to exhibit ferromagnetism down to the monolayer limit, whereas VBr_3 [11–13], $CrCl_3$ [14], and α-$RuCl_3$ [15] are antiferromagnetic at low temperatures. All these materials share a common structural motif of edge-sharing TX_6 octahedra forming a honeycomb lattice within the plane. Weak interlayer van der Waals interaction enables mechanical exfoliation down to the monolayer, making these materials ideal platforms for exploring two-dimensional magnetism and related phenomena [16,17].

Notably, unlike Cr^{3+} ions with a $3d^3$ electronic configuration, V^{3+} ions in vanadium trihalides possess a $3d^2$ configuration with an unquenched orbital angular momentum ($L = 1$), resulting in stronger spin-orbit coupling [6,18–20]. This enhanced coupling suggests a heightened sensitivity of vanadium trihalides to external stimuli such as strain and chemical substitution [21,22], offering promising opportunities for tuning their magnetic and electronic properties via physical or chemical means.

VCl_3 is a newly synthesized member of the vanadium trihalide family, crystallizing in the same BiI_3-type structure (space group $R\bar{3}$, No. 148) as VBr_3 and VI_3 at room temperature [23,24]. Unlike VI_3, which undergoes two structural phase transitions at $T_{S1} = 79$ K and $T_{S2} = 32$ K [6], VCl_3 exhibits a single structural transition at a slightly higher temperature [$T_S = 103.7(5)$ K], resembling the behavior of VBr_3 ($T_S = 90.4$ K) [11]. VCl_3 also parallels VBr_3 in magnetism, which orders antiferromagnetically below $T_N = 26.5$ K [11]. VCl_3 undergoes a similar transition into an antiferromagnetic ground state at $T_N = 21.8(1)$ K. In this paper, we present a comprehensive investigation of the structural and magnetic properties of bulk VCl_3 single crystals through neutron diffraction and thermodynamic measurements.

II. METHOD

Single crystals of VCl_3 were synthesized by chemical vapor transport. The commercially obtained VCl_3 precursor contained trace oxide-related impurities. To improve phase

*Contact author: zhaoj@fudan.edu.cn

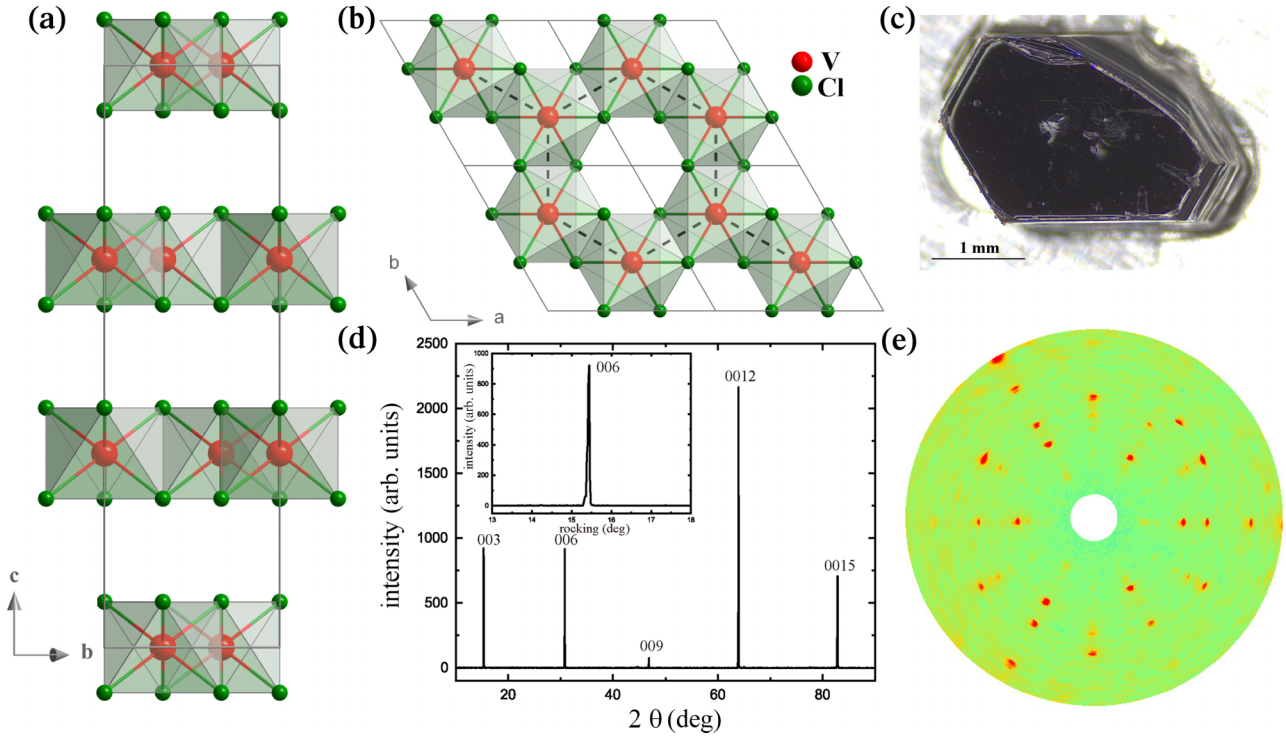

FIG. 1. Schematic illustrations of the crystal structure of VCl_3 viewed along the (a) *a* axis and (b) *c* axis. (c) Photograph of a high-quality VCl_3 single crystal. (d) X-ray diffraction pattern of the cleaved surface measured at room temperature. The inset shows the rocking curve of the (0, 0, 6) reflection. (e) X-ray Laue diffraction pattern taken along the *c* axis.

purity, the starting material was first subjected to a vacuum-sealed purification treatment under reducing conditions to suppress residual oxide phases. The resulting powder was subsequently sealed in a quartz tube under vacuum and placed in a horizontal three-zone furnace. The hot end was maintained at 550 °C, while the cold end was kept at 480 °C for 21 days, followed by slow cooling to room temperature. Large hexagonal sheetlike VCl_3 single crystals formed at the cold end of the quartz tube. Similar to its sister compounds VBr_3 and VI_3, VCl_3 rapidly absorbs moisture from the air and undergoes oxidation and degradation. Therefore, all sample handling was conducted in a glovebox under an inert gas atmosphere.

The high quality of the sample was verified by a high-resolution D8 Discover x-ray diffractometer equipped with a copper x-ray source from Bruker. We conducted heat capacity, magnetic susceptibility, and magnetization measurements on VCl_3 single crystals using a 9-T physical property measurement system (Quantum Design) and 7-T magnetic property measurement system (Quantum Design). The high-field magnetization measurements were performed at the Steady High Magnetic Field Facility (SHMFF) of the High Magnetic Field Laboratory. The pulsed field measurements were performed at Wuhan National High Magnetic Field Center.

To determine the magnetic and nuclear structures, we performed single-crystal neutron diffraction experiments using the four-cycle mode of the Dimensional Extreme Magnetic Neutron Diffractometer (DEMAND, HB-3A) at the High Flux Isotope Reactor at Oak Ridge National Laboratory [25]. The single crystal used in this experiment was about 2 mm in diameter and 0.5 mm thick and weighed about 5 mg. The crystal was cooled down to the base temperature of 5 K using a closed-cycle refrigerator. The neutron wavelength used was 1.533 Å. In addition, single-crystal neutron diffraction measurements were also carried out on the time-of-flight diffractometer wide angle in a single histogram (WISH) [26] at the ISIS Neutron and Muon Source. A single crystal of around 14 mg was used for this experiment. Diffraction data were reduced using mantid software [27]. The nuclear and magnetic structures were refined using the fullprof suite [28].

III. RESULTS AND DISCUSSION

The structure of VCl_3 is illustrated in Figs. 1(a) and 1(b). Each V^{3+} ion is octahedrally coordinated by six Cl^- ions, forming edge-sharing VCl_6 octahedra within the plane. The as-grown single crystals exhibit a dark, sheetlike morphology with well-defined natural edges, characteristic of their layered nature [Fig. 1(c)]. Our crystals are relatively large and exhibit well-defined natural edges, which make possible a wider range of measurements, including single-crystal neutron diffraction. The presence of sharp 00*l* Bragg reflections in the x-ray diffraction pattern [Fig. 1(d)] confirms the high crystallinity of the sample. The x-ray Laue diffraction pattern taken along the *c* axis [Fig. 1(e)] further reveals a clear threefold rotational symmetry.

A structural phase transition is confirmed by a distinct anomaly in the heat capacity at $T_S = 103.7(5)$ K [Fig. 2(a)]. Magnetic susceptibility measurements with fields along the *c* axis and within the *ab* plane reveal a clear kink and anisotropic splitting [Fig. 3(a)], also indicating the structural phase tran-

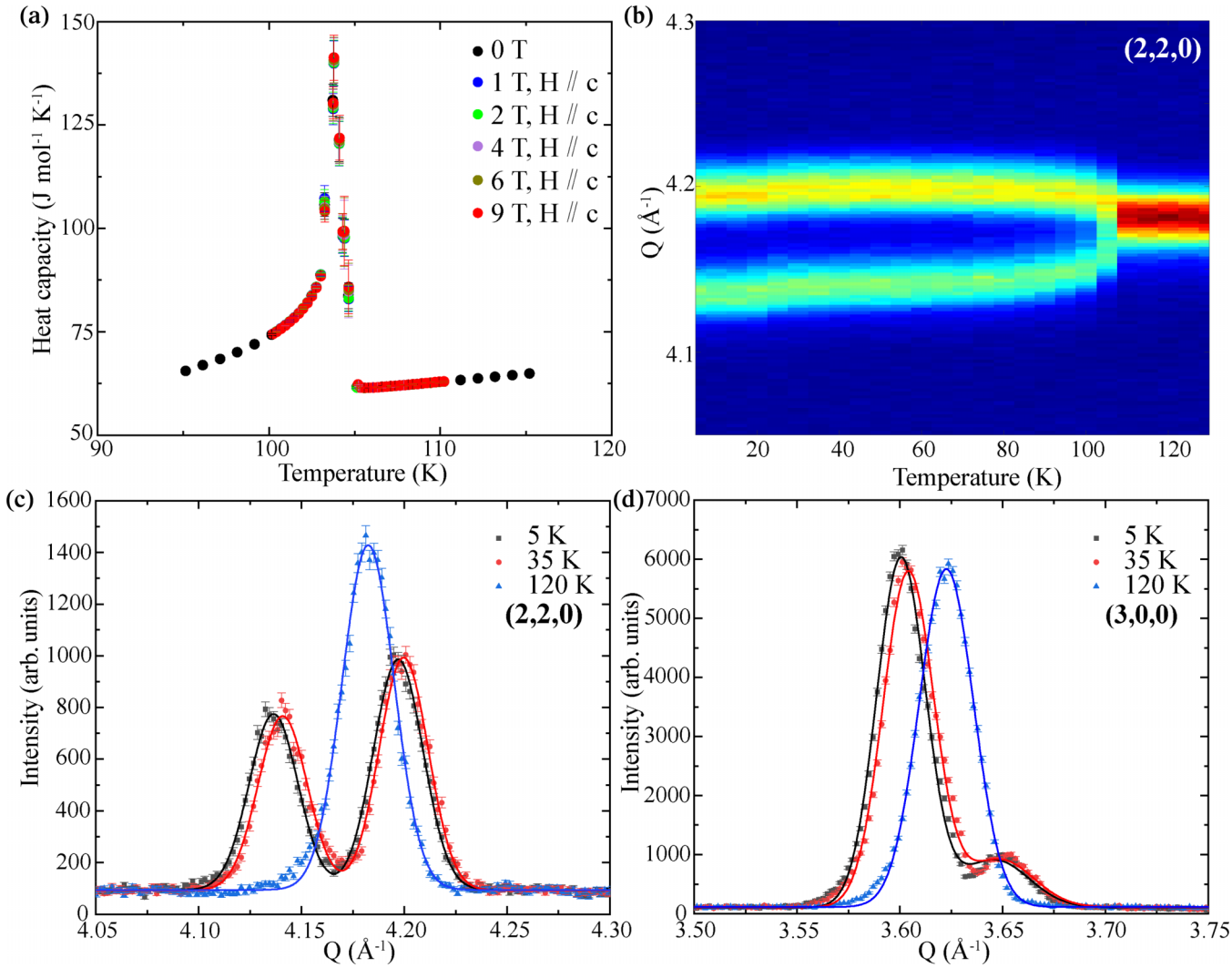

FIG. 2. Structural phase transition at $T_S = 103.7(5)$ K in VCl_3. (a) Heat capacity measured from 95 to 115 K as a function of temperature. (b) Temperature dependence of the Bragg peak (2, 2, 0). The heat map was generated using raw data from scans of the (2, 2, 0) peak at temperatures ranging from 5 to 130 K with an interval of 5 K. (c) and (d) Comparison of selected in-plane Bragg peaks at different temperatures, showing clear peak splitting associated with the structural distortion.

sition. To investigate this transition in greater detail, we performed single-crystal neutron diffraction measurements at DEMAND, HB-3A. Nuclear Bragg peaks of the (2, 2, 0) reflection were measured at various temperatures to track the structural evolution. At $T = 120$ K, the nuclear peaks are well indexed by a rhombohedral lattice with lattice parameters $a = b = 6.0082(5)$ Å and $c = 17.3373(30)$ Å (in hexagonal notation), consistent with previous reports [29]. Upon cooling through the structural transition at $T_S = 103.7(5)$ K, a clear splitting of the (2, 2, 0) Bragg peak emerges [Fig. 2(b)]. Comparisons of selected Bragg reflections at different temperatures are shown in Figs. 2(c) and 2(d). From the measured Bragg peaks, the in-plane lattice constants at 5 K are determined to be 6.0451(4) Å and 5.9697(4) Å. The observed ~1.2% change in the in-plane lattice constant suggests that the structural phase transition breaks the threefold rotational (C_3) symmetry. No appreciable difference is observed between the 5 and 35 K datasets, indicating the absence of additional structural transitions at lower temperatures. This behavior closely resembles that of VBr_3, in contrast to VI_3, which exhibits two distinct structural transitions [6,11]. The proximity of the split in the lattice peaks, combined with the intrinsic crystal quality limitations of van der Waals materials, makes it difficult to index structural peaks and refine the nuclear structure at low temperature. However, the splitting of in-plane Bragg peaks provides a direct measure of the relative volume fractions of domains. By analyzing the integrated intensities of the split Bragg reflections, we estimate the volume ratio of the different structural domains in this crystal to be 5:4:1. The imbalance of the domain volumes may be related to the preexisting structure strains formed during the crystal's growth.

We now turn to the magnetic properties of VCl_3. Magnetic susceptibility and heat capacity measurements at low temperatures reveal a clear antiferromagnetic phase transition at $T_N = 21.8(1)$ K [Figs. 3(a) and 3(c)]. The transition temperature is progressively suppressed by an applied magnetic field, with a more rapid reduction for fields along the c axis than for fields within the ab plane [Figs. 3(c) and 3(d)].

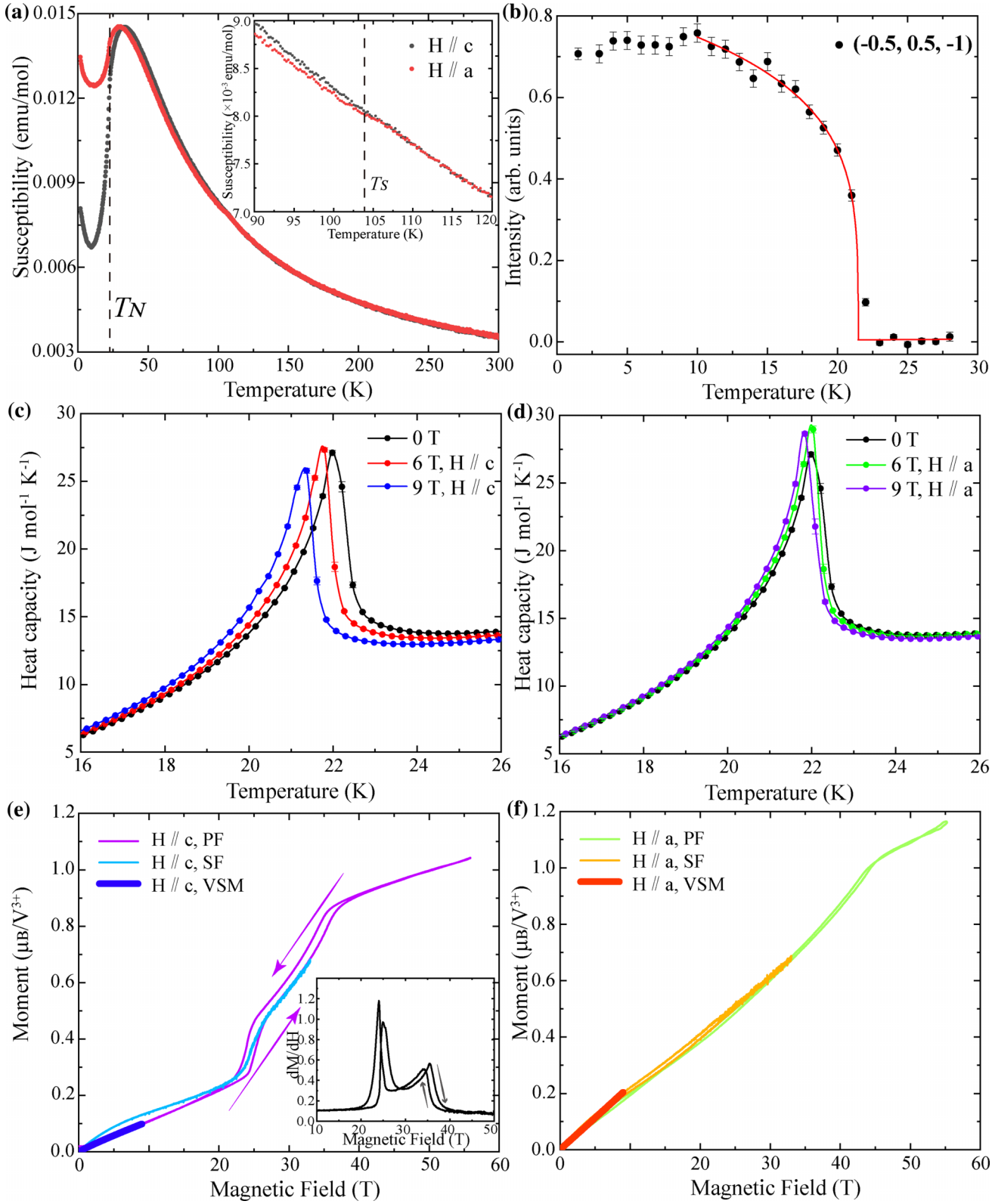

FIG. 3. Magnetic phase transition at $T_N = 21.8(1)$ K in VCl_3. (a) Magnetic susceptibility measured from 1.8 to 300 K under an external field of 500 Oe. The inset provides a zoomed-in view of the structural phase transition. (b) Temperature dependence of the intensity of the magnetic Bragg peak (−0.5, 0.5, −1), as measured by neutron diffraction on WISH, ISIS. The red line is a fit using the critical power law $I \sim (1-T/T_N)^{2\beta}$. Low-temperature heat capacity under external magnetic fields along the (c) *c* axis and (d) *a* axis. Magnetization curve obtained from laboratory-based vibrating sample magnetometry (VSM), steady high magnetic field measurements (SF), and pulsed field experiments (PF) under external magnetic fields along the (e) *c* axis and (f) *a* axis. The inset of (e) shows the raw derivative data from the pulsed field measurement, where a clear two-step transition is observed.

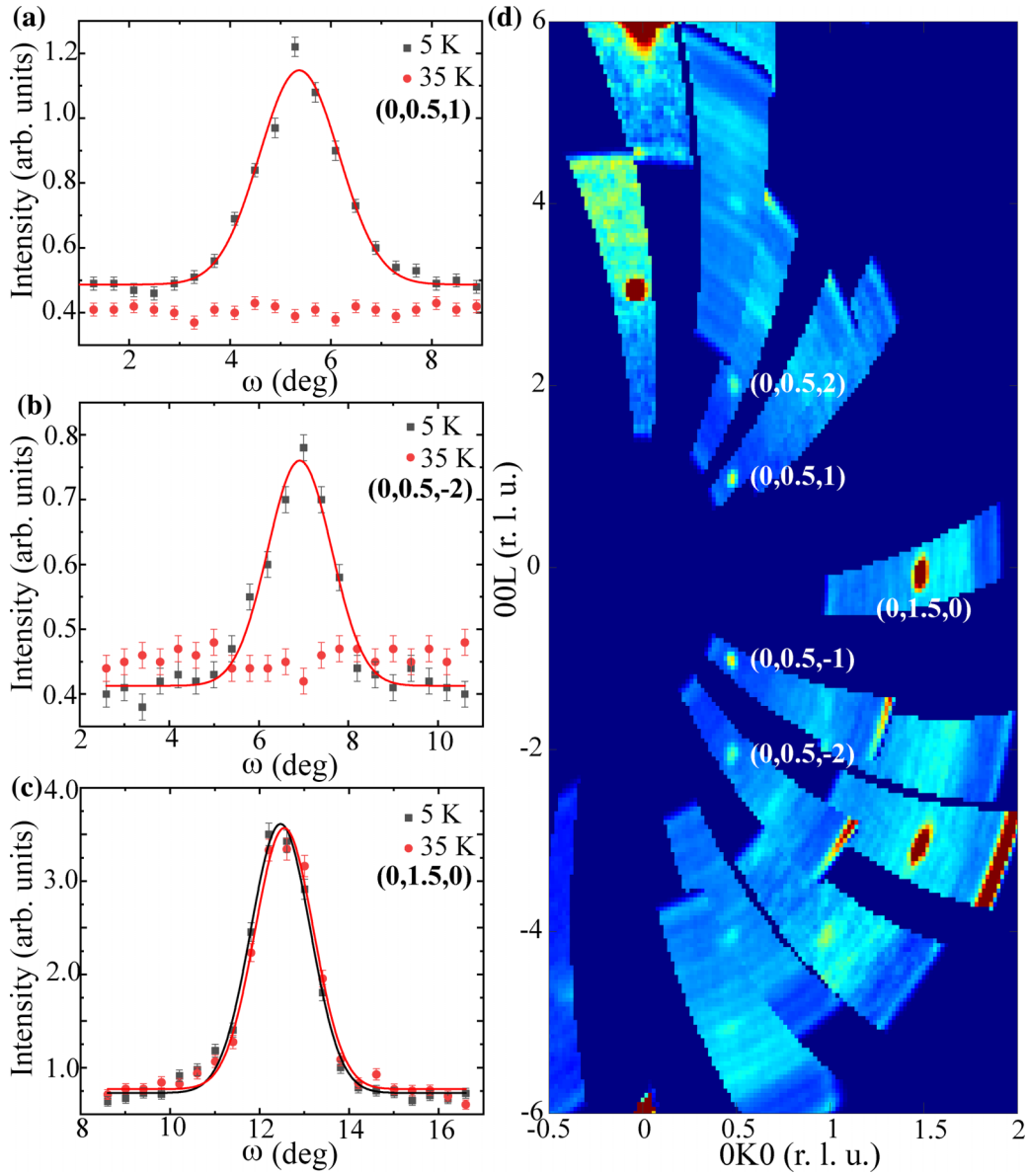

FIG. 4. (a) and (b) A high- and low-temperature comparison of two representative inequivalent magnetic Bragg peaks, highlighting the emergence of magnetic intensity at low temperature. (c) Temperature comparison of the (0, 1.5, 0) peak, which shows negligible change, indicating that the signal is a spurious reflection arising from half-wavelength neutrons rather than a magnetic origin. (d) Neutron diffraction mapping of the (0, K, L) reciprocal plane at the base temperature obtained on HB-3A, ORNL, revealing a distinct set of magnetic Bragg peaks.

Field-dependent magnetization measurements also reveal anisotropic behavior [Figs. 3(e) and 3(f)]. The data from the pulsed field and the steady high magnetic field are calibrated based on the vibrating sample magnetometry (VSM) data since the VSM measures an absolute value. For a magnetic field applied along the a axis, the magnetization increases linearly and exhibits a distinct change in slope at approximately 44 T. In contrast, for the field applied along the c axis, the magnetization displays two steplike transitions at 25.2 and 35.4 T during the up-sweep, which shift to 24.0 and 34.2 T upon the down-sweep, indicating hysteresis. These transitions appear as two pronounced peaks in the differential pulsed field magnetization raw data [see the inset of Fig. 3(e)], implying field-induced anomalies in the magnetization process. Between these transitions, the magnetization shows a markedly reduced slope, suggesting the presence of an intermediate field regime with plateaulike behavior near half magnetization.

To gain microscopic insight into the observed macroscopic magnetic behavior, we performed single-crystal neutron diffraction measurements on VCl_3. Since the structural distortion across the transition is relatively minor, all magnetic structure analyses were conducted based on the high-symmetry $R\bar{3}$ phase. Upon cooling below $T_N = 21.8(1)$ K, additional Bragg peaks emerge at half-integer positions in reciprocal space, indexed by the magnetic propagation vector $k = (0, 0.5, 1)$ in hexagonal notation. Figures 4(a) and 4(b) compare the temperature dependence of two representative magnetic reflections, (0, 0.5, 1) and (0, 0.5, −2). Figure 4(c) shows a comparison of the (0, 1.5, 0) reflection at high and low temperatures, with no significant

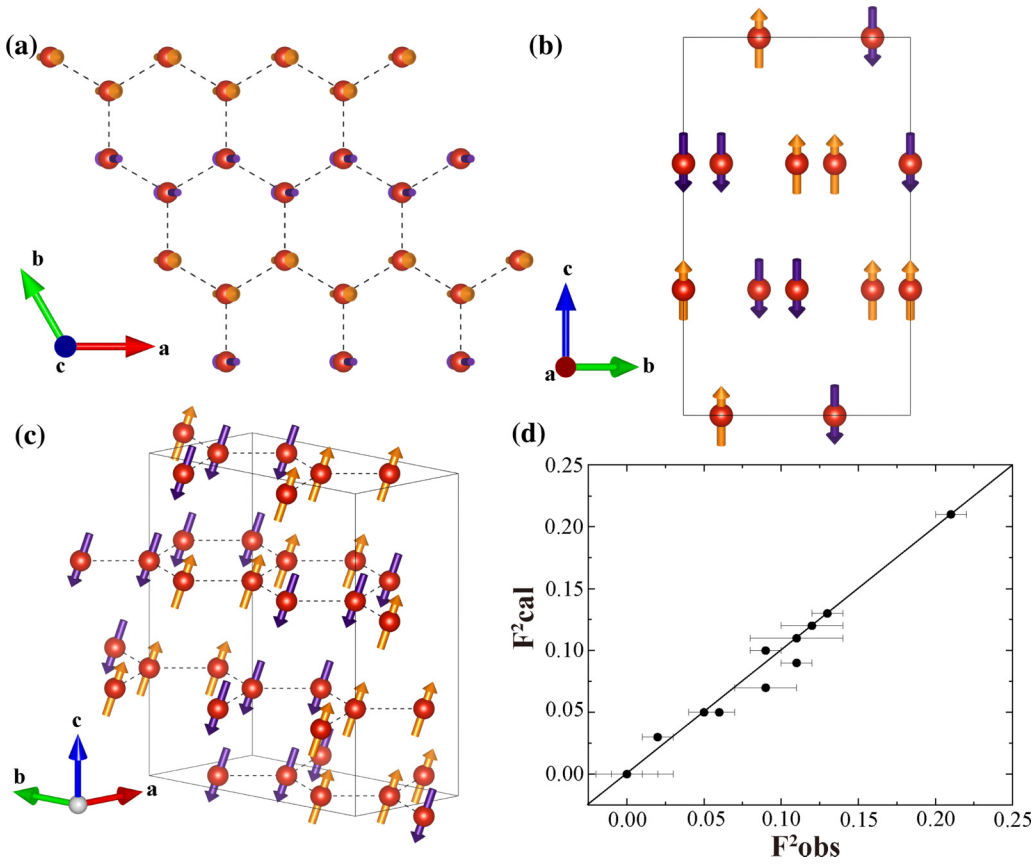

FIG. 5. Magnetic structure of VCl_3. Schematic views of the refined magnetic structure projected along the (a) c axis and (b) a axis. (c) Overall illustration of the zigzag antiferromagnetic structure of VCl_3 as determined by least squares refinement. (d) Comparison of the observed magnetic structure factors and those calculated from the refined model. The resulting reliability factor, RF = 5.23, indicates a good quality of fit.

difference observed, indicating that this signal arises from half-wavelength neutrons ($\lambda/2$ contamination) rather than a magnetic origin. Using the determined propagation vector and the rhombohedral crystal structure, we performed symmetry analysis with the Bilbao Crystallographic Server [30–33] and simulated annealing and representation analysis (SARAh) [34]. The magnetic representation can be decomposed as $\Gamma_{\text{Mag}} = 3\Gamma_1^1 \oplus 3\Gamma_2^1$. Each irreducible representation contributes three independent basis vectors. The three basis vectors of Γ_1^1 correspond to spin configurations in which the two magnetic sublattices are coupled antiferromagnetically, giving rise to a zigzag-type order. In contrast, the three basis vectors of Γ_2^1 correspond to configurations in which the sublattices are aligned parallel along the respective directions, resulting in a stripe-type order. Both configurations belong to magnetic space group $P_s\bar{1}$. The absence of magnetic Bragg intensity at (0, 1.5, 0) and its symmetry-equivalent positions rules out the stripe configuration, thereby identifying the zigzag magnetic order as the ground state of VCl_3. Figure 4(d) displays an extended map of reciprocal space at the base temperature, showing both magnetic and nuclear Bragg peaks. The temperature dependence of the $(-0.5, 0.5, -1)$ reflection, which is symmetry equivalent to (0, 0.5, 1), is shown in Fig. 3(b), and it clearly indicates a magnetic phase transition at about 22 K, consistent with the behavior observed in heat capacity and susceptibility measurements. The critical power law fit $I \sim (1-T/T_N)^{2\beta}$ yields a critical exponent $\beta = 0.130$, which is close to the 2D limit ($\beta = 0.125$).

In compounds such as VCl_3 and VBr_3, lattice distortion at low temperatures gives rise to three distinct structural domains, each rotated by 120° with respect to one another. In our single crystal, upon cooling below T_S, the population of these domains is slightly different, resulting in different scale factors for each domain. This domain imbalance is evident in our neutron diffraction data, where the intensity of a given magnetic Bragg peak varies between domains and shows a one-to-one correspondence with the intensity of the associated structural Bragg peaks. These observations confirm the presence of multiple structural domains with unequal contributions and allow us to exclude the possibility of a triple-Q magnetic structure, as recently proposed in other honeycomb magnets such as $Na_2Co_2TeO_6$ [35].

Furthermore, the relative population of each structural domain formed upon cooling below T_N can be estimated from the intensity ratios of selected magnetic Bragg peaks. By incorporating the corresponding scale factors obtained from structural refinement, we carried out magnetic structure refinement and determined the ordered moment components to be $M_z = 1.02(3)\mu_B$, $M_x = 0.40(3)\mu_B$, and $M_y = 0.00(2)\mu_B$. The total ordered moment is $M_{\text{tot}} = 1.09(2)\mu_B$. This value agrees well with the moment inferred from magnetization measurements [Figs. 3(e) and 3(f)]. The total ordered moment

is also smaller than the theoretical spin-only value for V^{3+} ($S = 1$), likely due to the presence of a substantial orbital contribution that partially cancels the spin moment, which is an effect similarly observed in VBr_3 and VI_3 [6,11]. Schematic representations of the refined magnetic structure are shown in Figs. 5(a)–5(c). The magnetic moments in VCl_3 lie within the *ac* plane and are predominantly oriented out of the *ab* plane. This configuration is consistent with the magnetic anisotropy observed in susceptibility measurements, where the residual susceptibility below T_N is smaller for fields applied along the *c*-axis direction [Fig. 3(a)].

Recent photoemission and first-principles studies revealed the existence of localized electron polarons in VCl_3, accompanied by local bond elongation and orbital reconstruction [24]. Such local lattice-orbital modulations can, in principle, modify the V–Cl–V hopping amplitudes and the orbital overlap and hence renormalize the superexchange interactions. Moreover, magnetization plateaus could be a hallmark of frustrated magnetism and have been reported in a wide variety of systems, including triangular-lattice antiferromagnets [36], kagome lattices [37], spinel chromates [38], and low-dimensional Ising-like magnets [39]. While the microscopic mechanisms differ, they share the feature of stabilizing commensurate spin configurations over finite field ranges, often through the combined effects of exchange frustration, anisotropy, and Zeeman energy. In VCl_3, the emergence of the magnetization plateau suggests the stabilization of a field-induced state distinct from both the zero-field zigzag order and the fully polarized state. One possible scenario involves partial spin reorientations among four neighboring zigzag chains, in which the system evolves from an up-down-up-down arrangement into an up-up-up-down configuration under an out-of-plane field. This type of configuration naturally gives rise to a fractional net moment and would be broadly analogous to collinear stacking sequences invoked to explain half plateaus in spinels and chain compounds [38]. Alternatively, the plateau phase in VCl_3 may not be strictly collinear. Noncollinear or canted arrangements could also yield the observed fractional magnetization if stabilized by anisotropic exchange interactions [40]. Given that strong bond-dependent Kitaev interactions have been reported in vanadium-based trihalides [41], it is plausible that similar exchange anisotropies are active in VCl_3. Such terms, in combination with interlayer coupling and conventional Heisenberg exchanges, could generate competing magnetic ground states and lead to plateau formation under a field. The possibility of a Kitaev-frustrated origin is particularly intriguing, as it would place VCl_3 among the rare systems in which fractional magnetization plateaus emerge from bond-anisotropic exchange rather than simple Ising-like stacking. To further elucidate the nature of this phase and the role of competing interactions in vanadium trihalides, more comprehensive investigations, particularly inelastic neutron scattering, are highly warranted.

IV. CONCLUSIONS

In summary, we synthesized large, high-quality single crystals of VCl_3 and investigated their structural and magnetic properties. Magnetic susceptibility and heat capacity measurements revealed a structural phase transition at $T_S = 103.7(5)\,\mathrm{K}$ and an antiferromagnetic transition at $T_N = 21.8(1)\,\mathrm{K}$, which were confirmed by neutron diffraction experiments. The magnetization curve along the *c* axis exhibits a plateaulike feature, indicative of unconventional field-dependent behavior. Neutron diffraction refinements further established the magnetic ground state as a zigzag antiferromagnetic order, with propagation vector $k = (0, 0.5, 1)$ in hexagonal notation. These findings place VCl_3 among the emerging family of vanadium-based trihalides that host diverse and nontrivial magnetic phenomena and provide a solid foundation for exploring their potential as model systems for correlated magnetism in low-dimensional lattices.

ACKNOWLEDGMENTS

This work was supported by the Key Program of the National Natural Science Foundation of China (Grant No. 12234006), the National Key R&D Program of China (Grant No. 2022YFA1403202), the Quantum Science and Technology-National Science and Technology Major Project (Grant No. 2024ZD0300103), the Shanghai Municipal Science and Technology Project (Grants No. 2019SHZDZX01 and No. 25DZ3008100), and the Large Scientific Facility Open Subject of Songshan Lake Laboratory (Grant No. KFKT2022A03). A portion of this research used resources at the High Flux Isotope Reactor, a DOE Office of Science User Facility operated by the Oak Ridge National Laboratory. The beam time was allocated to HB-3A DEMAND on Proposal No. IPTS-33274.1. We thank the staff members of the WM5 at the Steady High Magnetic Field Facility, CAS, for providing technical support and assistance in data collection and analysis. The authors thank the Science and Technology Facilities Council (UK) for the allocation of beam time on the WISH diffractometer (RB2420057). The raw data for the WISH experiment are available from [42].

DATA AVAILABILITY

The data that support the findings of this article are not publicly available upon publication because it is not technically feasible and/or the cost of preparing, depositing, and hosting the data would be prohibitive within the terms of this research project. The data are available from the authors upon reasonable request.

[1] K. S. Burch, D. Mandrus, and J. G. Park, Magnetism in two-dimensional van der Waals materials, Nature (London) **563**, 47 (2018).

[2] C. Gong, L. Li, Z. Li, H. Ji, A. Stern, Y. Xia, T. Cao, W. Bao, C. Wang, Y. Wang, Z. Q. Qiu, R. J. Cava, S. G. Louie, J. Xia, and X. Zhang, Discovery of intrinsic ferromagnetism in

two-dimensional van der Waals crystals, Nature (London) **546**, 265 (2017).

[3] D. L. Duong, S. J. Yun, and Y. H. Lee, van der Waals layered materials: Opportunities and challenges, ACS Nano **11**, 11803 (2017).

[4] M. Gibertini, M. Koperski, A. F. Morpurgo, and K. S. Novoselov, Magnetic 2D materials and heterostructures, Nat. Nanotechnol. **14**, 408 (2019).

[5] S. Kumari, D. K. Pradhan, N. R. Pradhan, and P. D. Rack, Recent developments on 2D magnetic materials: Challenges and opportunities, Emergent Mater. **4**, 827 (2021).

[6] Y. Hao, Y. Gu, Y. Gu, E. Feng, H. Cao, S. Chi, H. Wu, and J. Zhao, Magnetic order and its interplay with structure phase transition in van der Waals ferromagnet VI_3, Chin. Phys. Lett. **38**, 096101 (2021).

[7] S. Son, M. J. Coak, N. Lee, J. Kim, T. Y. Kim, H. Hamidov, H. Cho, C. Liu, D. M. Jarvis, P. A. C. Brown, J. H. Kim, C.-H. Park, D. I. Khomskii, S. S. Saxena, and J.-G. Park, Bulk properties of the van der Waals hard ferromagnet VI_3, Phys. Rev. B **99**, 041402(R) (2019).

[8] T. Kong, K. Stolze, E. I. Timmons, J. Tao, D. Ni, S. Guo, Z. Yang, R. Prozorov, and R. J. Cava, VI_3—A new layered ferromagnetic semiconductor, Adv. Mater. **31**, 1808074 (2019).

[9] M. A. McGuire, H. Dixit, V. R. Cooper, and B. C. Sales, Coupling of crystal structure and magnetism in the layered, ferromagnetic insulator CrI_3, Chem. Mater. **27**, 612 (2015).

[10] B. Huang, G. Clark, E. Navarro-Moratalla, D. R. Klein, R. Cheng, K. L. Seyler, D. Zhong, E. Schmidgall, M. A. McGuire, D. H. Cobden, W. Yao, D. Xiao, P. Jarillo-Herrero, and X. Xu, Layer-dependent ferromagnetism in a van der Waals crystal down to the monolayer limit, Nature (London) **546**, 270 (2017).

[11] Y. M. Gu, Y. Q. Hao, Z. Y. Kao, Y. Gu, F. Liu, S. Zheng, H. Cao, L. He, and J. Zhao, Lattice and magnetic structure in the van der Waals antiferromagnet VBr_3, Phys. Rev. B **110**, 064403 (2024).

[12] T. Kong, S. Guo, D. Ni, and R. J. Cava, Crystal structure and magnetic properties of the layered van der Waals compound VBr_3, Phys. Rev. Mater. **3**, 084419 (2019).

[13] B. B. Lyu, L. Wang, Y. F. Gao, S. Guo, X. Zhou, Z. Hao, S. Wang, Y. Zhao, L. Huang, J. Shao, and M. Huang, Structural and magnetic phase transitions in quasi-two-dimensional VBr_3, Phys. Rev. B **106**, 085430 (2022).

[14] B. Kuhlow, Magnetic ordering in $CrCl_3$ at the phase transition, Phys. Status Solidi A **72**, 161 (1982).

[15] H. B. Cao, A. Banerjee, J. Q. Yan, C. A. Bridges, M. D. Lumsden, D. G. Mandrus, D. A. Tennant, B. C. Chakoumakos, and S. E. Nagler, Low-temperature crystal and magnetic structure of α-$RuCl_3$, Phys. Rev. B **93**, 134423 (2016).

[16] D. Hovančík, M. Kratochvílová, T. Haidamak, P. Doležal, K. Carva, A. Bendová, J. Prokleška, P. Proschek, M. Míšek, D. I. Gorbunov, J. Kotek, V. Sechovský, and J. Pospíšil, Robust intralayer antiferromagnetism and tricriticality in the van der Waals compound VBr_3, Phys. Rev. B **108**, 104416 (2023).

[17] Y. Li, B. Yang, S. Xu, B. Huang, and W. Duan, Emergent phenomena in magnetic two-dimensional materials and van der Waals heterostructures, ACS Appl. Electron. Mater. **4**, 3278 (2022).

[18] D. Hovancik, J. Pospisil, K. Carva, V. Sechovsky, and C. Piamonteze, Large orbital magnetic moment in VI_3, Nano Lett. **23**, 1175 (2023).

[19] H. Lane, E. Pachoud, J. A. Rodriguez-Rivera, M. Songvilay, G. Xu, P. M. Gehring, J. P. Attfield, R. A. Ewings, and C. Stock, Two-dimensional ferromagnetic spin-orbital excitations in honeycomb VI_3, Phys. Rev. B **104**, L020411 (2021).

[20] A. De Vita, T. T. P. Nguyen, R. Sant, G. M. Pierantozzi, D. Amoroso, C. Bigi, V. Polewczyk, G. Vinai, L. T. Nguyen, T. Kong, J. Fujii, I. Vobornik, N. B. Brookes, G. Rossi, R. J. Cava, F. Mazzola, K. Yamauchi, S. Picozzi, and G. Panaccione, Influence of orbital character on the ground state electronic properties in the van der Waals transition metal iodides VI_3 and CrI_3, Nano Lett. **22**, 7034 (2022).

[21] L. Liu, K. Yang, G. Wang, and H. Wu, Two-dimensional ferromagnetic semiconductor VBr_3 with tunable anisotropy, J. Mater. Chem. C **8**, 14782 (2020).

[22] P. Kumari, T. Mukherjee, S. Kar, and S. J. Ray, $VClBr_2$: A new two-dimensional (2D) ferromagnetic semiconductor, J. Appl. Phys. **133**, 183901 (2023).

[23] M. Kratochvilova, P. Dolezal, D. Hovancik, J. Pospisil, A. Bendova, M. Dusek, V. Holy, and V. Sechovsky, Crystal structure evolution in the van der Waals vanadium trihalides, J. Phys.: Condens. Matter **34**, 294007 (2022).

[24] D. Mastrippolito, L. Camerano, H. Świątek, B. Šmíd, T. Klimczuk, L. Ottaviano, and G. Profeta, Polaronic and Mott insulating phase of layered magnetic vanadium trihalide VCl_3, Physi. Rev. B **108**, 045126 (2023).

[25] H. Cao, B. C. Chakoumakos, K. M. Andrews, Y. Wu, R. A. Riedel, J. Hodges, W. Zhou, R. Gregory, B. Haberl, J. Molaison, and G. W. Lynn, DEMAND, a dimensional extreme magnetic neutron diffractometer at the high flux isotope reactor, Crystals **9**, 5 (2019).

[26] L. C. Chapon, P. Manuel, P. G. Radaelli, C. Benson, L. Perrott, S. Ansell, N. J. Rhodes, D. Raspino, D. Duxbury, E. Spill, and J. Norris, Wish: The new powder and single crystal magnetic diffractometer on the second target station, Neutron News **22**, 22 (2011).

[27] O. Arnold, *et al.*, Mantid—Data analysis and visualization package for neutron scattering and μSR experiments, Nucl. Instrum. Methods. Phys. Res. Sect. A **764**, 156 (2014).

[28] J. Rodriguez-Carvajal, Recent advances in magnetic-structure determination by neutron powder diffraction, Phys. B (Amsterdam, Neth.) **192**, 55 (1993).

[29] W. Klemm and E. Krose, Die Kristallstrukturen von $ScCl_3$, $TiCl_3$ und VCl_3, Z. Anorg. Chem. **253**, 218 (2004).

[30] M. I. Aroyo, J. M. Perez-Mato, C. Capillas, E. Kroumova, S. Ivantchev, G. Madariaga, A. Kirov, and H. Wondratschek, Bilbao Crystallographic Server: I. Databases and crystallographic computing programs, Z. Kristallogr. **221**, 15 (2006).

[31] M. I. Aroyo, A. Kirov, C. Capillas, J. M. Perez-Mato, and H. Wondratschek, Bilbao Crystallographic Server. II. Representations of crystallographic point groups and space groups, Acta Crystallogr. Sect. A **62**, 115 (2006).

[32] J. M. Perez-Mato, S. V. Gallego, E. S. Tasci, L. Elcoro, G. de la Flor, and M. I. Aroyo, Symmetry-based computational tools for magnetic crystallography, Annu. Rev. Mater. Res. **45**, 217 (2015).

[33] V. Petrícek, J. Fuksa, and M. Dusek, Magnetic space and superspace groups, representation analysis: Competing or friendly concepts? Acta Crystallogr. Sect. A **66**, 649 (2010).

[34] A. S. Wills, A new protocol for the determination of magnetic structures using simulated annealing and representational analysis (SARAh), Phys. B (Amsterdam, Neth.) **276–278**, 680 (2000).

[35] W. Yao, Y. Zhao, Y. Qiu, C. Balz, J. R. Stewart, J. W. Lynn, and Y. Li, Magnetic ground state of the Kitaev $Na_2Co_2TeO_6$ spin liquid candidate, Phys. Rev. Res. **5**, L022045 (2023).

[36] R. Okuma, C. Ritter, G. J. Nilsen, and Y. Okada, Magnetic frustration in a van der Waals metal CeSiI, Phys. Rev. Mater. **5**, L121401 (2021).

[37] T. Matsuda, S. Partzsch, T. Tsuyama, E. Schierle, E. Weschke, J. Geck, T. Saito, S. Ishiwata, Y. Tokura, and H. Wadati, Observation of a devil's staircase in the novel spin-valve system $SrCo_6O_{11}$, Phys. Rev. Lett. **114**, 236403 (2015).

[38] N. Shannon, H. Ueda, Y. Motome, K. Penc, H. Shiba, and H. Takagi, Half-magnetization plateaux in Cr spinels, J. Phys.: Conf. Ser. **51**, 31 (2006).

[39] A. Devillez, J. Robert, E. Lhotel, R. Ballou, C. Cavenel, F. Denis Romero, Q. Faure, H. Jacobsen, J. Lass, D. G. Mazzone, U. Bengaard Hansen, M. Enderle, S. Raymond, S. De Brion, V. Simonet, and M. Songvilay, Bond-dependent interactions and ill-ordered state in the honeycomb cobaltate $BaCo_2(AsO_4)_2$, Phys. Rev. Res. **7**, L042040 (2025).

[40] Z. Chen, B. Zhang, W. Zhu, L. Li, B. Liu, J. Feng, C. Xu, and H. Xiang, Strength of Kitaev interaction in $Na_3Co_2SbO_6$ and $Na_3Ni_2BiO_6$, Sci. China Phys. Mech.Astron. (2025).

[41] Y. Gu, Y. Gu, F. Liu, S. Ohira-Kawamura, N. Murai, and J. Zhao, Signatures of Kitaev interactions in the van der Waals ferromagnet VI_3, Phys. Rev. Lett. **132**, 246702 (2024).

[42] Z. Kao, *et al.*, The magnetic structure of a new van der Waals magnet, STFC ISIS Neutron and Muon Source (2024), https://doi.org/10.5286/ISIS.E.RB2420057.